Spatially-resolved metabolomic identifies colibactin-specific principles of reprogrammed lipid metabolism to promote cancer progression

Nilmara de Oliveira Alves[1], Olivier Boulard[1], Amaury Vaysse[2], Guillaume Dalmasso[3], Darja Nikitina[4], Richard Ruez[1], Thierry Pedron[5], Emma Bergstein[2], Pierre Sauvanet[3], Diane Letourneur[2], Catherine Godfraind[3], Imène Najjar[2], Emmanuel Lemichez[6], Juan Lucio Iovanna[7], Denis Mestivier[8], Nicolas Barnich[3], Philippe Sansonetti[5], Christophe Malabat[2], Marc Monot[2], Sean Kennedy[4], Amel Mettouchi[6], Richard Bonnet[3], Iradj Sobhani[6,8], Mathias Chamaillard[1]

[1] ONCOLillle, INSERM, U1003, Lille, France

[2] Institute Pasteur, Department of Computational Biology, Paris, France

[3] University of Clermont Auvergne, INSERM, UMR 1071, Clermont-Ferrand, France

[4] Institute Pasteur, USR3756, CNRS, Paris, France

[5] Institut Pasteur, Inserm, U1202, Paris, France.

[6] Institut Pasteur, CNRS, UMR 2001, Paris, France

[7] Centre de Recherche en Cancérologie de Marseille, INSERM U1068, CNRS UMR 7258, Institut Paoli-Calmettes, Aix-Marseille Université, Marseille, France

[8] Université Paris Est Créteil, EA7375 – EC2M, Créteil, France

To whom correspondence should be addressed: mathias.chamaillard@inserm.fr

ABSTRACT

The cellular heterogeneity within a variety of solid tumors is influenced by several type of tumor-associated bacteria through yet poorly understood mechanisms. Unbiased genomic analysis revealed that right-sided colorectal tumors with poorer prognosis are preferentially populated with species related to *Escherichia coli*, including strains that are producing colibactin. By applying metabolomic profiling *in situ*, the presence of colibactin-producing *Escherichia coli* (CoPEC) was identified to establish a high-glycerophospholipid microenvironment within right-sided colorectal tumors that are bearing mutations in either APC or KRAS. Using spatial approaches, we revealed that bacterial microniches are poorly infiltrated with $CD8^+$ T cells. The aforementioned alterations in lipid metabolism negatively correlated with immunomodulatory and neurotrophic factors among which the human regenerating family member 3 alpha gene (REG3A). Accordingly, the loss of its ortholog enhances growth at the proximal colon of tumors with a microenvironment that impedes immune surveillance and shares similarities to human right-sided colorectal tumors. This work clarifies how the presence of colibactin-producing bacteria may locally establish tumor heterogeneity for lipid metabolism to promote cancer progression and provide unique insights both for therapeutic intervention and enabling basic research into the mechanisms of microbiota-host interaction.

STATEMENT OF SIGNIFICANCE: Applying *in situ* metabolic imaging to patients' tumors revealed that the accumulation of colibactin-producing bacteria that locally creates a potential vulnerability to cancer treatments through lipid metabolic reprogramming of tumor cells.

INTRODUCTION

Colorectal cancer (CRC) is the second most common form of malignancy and cancer-related death worldwide (1). Patients with right-sided colon cancer (RCC) have a worse prognosis than left-sided colon cancer (LCC) and it has already been reported that they do not respond well to conventional chemotherapies (2). Besides inter-individual heterogeneity, distinct tumor cell types within the same tumor have been identified but their origin remains elusive (3). Only recently has been established that some bacteria populate specific niches within the tumor microenvironment that impede immune surveillance and may subsequently promote tumor persistence (4). Importantly, disturbances in the gut microbial are associated with altered lipid metabolism, which can contribute to tumor resistance (5,6).

Escherichia coli bacteria are constitutive members of the human gut microbiota. However, colibactin-producing *Escherichia coli* (CoPEC) may promote colon tumor growth by modifying the tumor microenvironment (7). It has been well established that CoPEC induces double-strand breaks (DSBs) (8) as well as generates DNA adducts in mammalian cells (9). Equally of importance, CRC patients colonized by CoPEC are associated with a decrease of tumor-infiltrating T lymphocytes and they suggest that the presence of this genotoxin promotes a procarcinogenic immune environment through impairment of antitumor T-cell response, leading to tumoral resistance to immunotherapy (10). Nevertheless, whether the presence of CoPEC contributes to tumor lipid metabolism remains incompletely understood.

Herein, we identified *Escherichia-Shigella* as a significant genus, increasing in relapse patients. Furthermore, we demonstrate that colonization by positive CoPEC is an unfavorable prognostic factor in RCC with a predominance of consensus molecular subtype 3 (metabolomic) and APC mutation. Given that the intratumoral microbiota has a heterogeneous distribution in tumor tissues, we used spatially resolved metabolic as a key tool to determine whether this local distribution correlated with distinct metabolic functions. Interestingly, spatial metabolomics and transcriptomics revealed a significant increase of glycerophospholipids and a lowered infiltration of CD8+ T cells in bacteria microniches, mainly in patients colonized by positive CoPEC.

Moreover, in a subgroup of RCC patients, we identified c-type lectin Reg3α (REG3A), a gene that encodes a C-type lectin antimicrobial peptide constitutively secreted in the gut lumen by Paneth cells, as a stem cell niche factor that modulates cancer progression (11). Notably, 72% of RCC patients with low REG3A expression are colonized by CoPEC. Interestingly, these patients showed a low PDL1 expression and will potentially be resistant to

immunotherapy. Furthermore, RCC patients with exacerbated glycerophospholipid intensity and low REG3A expression display an increase in immunoglobulins (Ig). Similarly, colon tumors from Reg3b-deficient (Reg3b$^{-/-}$) mice confirm an increase of mRNAs encoding Ig heavy and light chains. Hence, colon cancer-derived Ig can play a critical modulatory effect on immune cells.

Taken together, our findings clarify how the presence of colibactin-producing bacteria may locally establish tumor heterogeneity for evading immune surveillance and provided new insights for further exploration of resistance mechanisms in response to glycerophospholipid accumulation.

RESULTS

Intra- and inter-tumor heterogeneity microbiota in right-sided colon cancer (RCC)

To explore heterogeneous intra- and inter-tumoral bacterial ecosystems we performed 16S rRNA gene sequencing from RCC tissue. PCoA projection of the data revealed two clusters based on study groups: healthy and relapse RCC patients. Adonis analysis showed significant differences between the two study groups both at genus and species taxonomic level (p value= 0.0066, F model = 2.35 and p value= 0.0034, F model = 2.23, respectively) (Figure 1A and 1B). Curiously, we identified the genus *Escherichia-Shigella* and the specie *Escherichia coli* increasing in relapse patients (Figures 1C and 1D). Based on these differences, we investigated if the presence of colibactin influences survival outcomes, particularly in patients with stage III and stage IV. Here, we found that RCC patients colonized by positive CoPEC are associated with poor progression free-survival (p=0.018) (Figure 1E). Besides, we performed an analysis of consensus molecular subtypes (CMS) based on the gene expression profile: CMS1 (immune), CMS2 (canonical), CMS3 (metabolic), and CMS4 (mesenchymal) and more than 50% of patients colonized by COPEC were classified as CMS3. These patients showed a predominance of APC mutation (Figure 1F).

Given that RCC survival in these patients has been linked to the presence of colibactin, we sought to verify if bacterial taxa are statically distinct between positive and negative CoPEC patients. Even though no significant difference in alpha diversity was observed between these groups, analysis of beta diversity revealed 35 bacterial taxa statically distinct. Along with the *Escherichia-Shigella* group, nine bacterial ASVs linked to *Prevotella 9*, four different *Bacteroides* species (*B. uniformis, B. fragilis, B. stercoris, B. salyersiae*), *Lachnoclostridium, Barnesiella,* and *Odoribacter splanchnicus* were significantly increased in the patients colonized by positive CoPEC. At the same time, we detected 24 bacteria taxa (one phylum,

one class, one order, three genera, three species, and 15 ASVs) that were significantly depleted in the positive CoPEC patients (Figure 1G). Next, we selected only patients from the CMS3 group and performed differential abundance analysis according to their CoPEC status. Similar to previous results, we detected six bacterial taxa enriched and 12 decreased in positive CoPEC positive patients. *B. uniformis* and *O. splanchnicus* as well as in the general cohort were increased in this same group. Additional bacteria, *Bacteroides plebeius, Desulfovibrio piger* and *Veillonella* were also increased (Supplementary Figure S1).

In situ RNA analysis exhibits an immunosuppressive effect of the tumor-associated bacterial microniches

A local immunosuppressive effect of tumor-associated bacteria has recently been established (4), but the underlying mechanisms remain elusive. Spatial transcriptomics provides an opportunity to comprehensively the role of target genes in the context of the tumor microenvironment (12,13). In this regard, using *in situ* hybridization (FISH) imaging, we visually confirmed the heterogeneous distribution of bacterial microniches in the RCC tissue, including *Escherichia coli* (Figure 2A).

To gain information if cell-type composition differences between positive and negative CoPEC patients were applied to both quanTIseq and EPIC to quantify the relative proportions of infiltrating immune cells of tumors from bulk RNA-seq. Of note, cytotoxic $CD8^+$ T cells proportion was distinct between positive and negative CoPEC patients, suggesting the heterogeneity of the immune microenvironment tumor associated with colibactin (Figure 2B). Given this, we sought to determine whether there is a difference in $CD8^+$ T cell infiltrates in intra-and inter-tumor areas annotated as positive or negative for bacteria. Based on RNAscope-FISH overlay images, we revealed that bacteria microniches are characterized by immunosuppressive effect with a decrease of tumor-infiltrating $CD8^+$ T cells, mainly in patients colonized by positive CoPEC (Figures 2C and 2D).

Spatial metabolomics reveals an increased glycerophospholipid in colibactin-associated tumor

Considering the heterogeneity of RCC tissue, we proposed a spatially resolved metabolomics approach to discover tumor-associated metabolites. First, we conducted an untargeted metabolomics analysis of 77 tissues from RCC patients using a high spectral resolution of the FTICR-MS. In particular, four differential metabolites in the tumor and adjacent normal tissue (kinetin riboside, N-acetylneuraminic acid, piperidine and phosphatidic

acid [PA]) were identified as potential biomarkers (Supplementary Figure S2). Among these, PA was revealed to have the strongest prognostic relevance for future interventions.

To explore if the bacteria microniches are associated with altered metabolism, spatially resolved metabolomics was undertaken on the 12 tissue samples. On each tissue, 3–13 specific regions of interest (ROI) were selected according to the FISH image (Figure 3A). This resulted in a total of 90 ROI with bacteria microniches and 86 ROI without bacteria. Given that the intratumoral microbiota has a heterogeneous distribution within individual tumor tissues, we sought to determine whether there is a difference in the metabolite's expression in the local bacteria-associated tumors. Here, we detected 14 up-regulated metabolites in ROI with bacteria compared to ROI without bacteria in positive CoPEC patients (Figure 3B). Moreover, comparisons between ROI with and without bacteria in negative CoPEC patients revealed 14 metabolites down and 13 over-expressed (Figure 3C). Specifically, 11 metabolites were found up-regulated only in patients colonized by positive CoPEC such as Benzenoids (n=1), Fatty Acyls (n=1), Glycerophospholipids (n=3), Organic acids (n=1), Organoheterocyclic (n=2), Sphingolipids (n=1) and Sterol Lipids (n=2)) (Supplementary Figure S3). In addition, metabolomic differential expression in ROI with bacteria microniches revealed 107 metabolites up-regulated and 12 metabolites down-regulated in the positive CoPEC compared with the negative CoPEC patients' group, where 40% are classified as lipids. Among those lipids identified, approximately 82% belong to the glycerophospholipids subclass such as: PA, phosphatidylcholine (PC), phosphatidylinositol (PI), phosphatidylethanolamine (PE), phosphatidylserine (PS), phosphatidylglycerol (PG) and others (Figure 3D).

By applying spatial approaches, we are able to quantify the areas of overlap between $CD8^+$ T cells and glycerophospholipids. Interestingly, we observed a significant correlation between the quantification of $CD8^+$ spots and PC intensity ($r= -0.56$, $p= 0.04$) in the positive CoPEC patients (Figure 3E). However, this correlation was lost in the negative CoPEC patients ($r=-0.04$, $p=0.81$) (Figure 3F). This result suggested that $CD8^+$ T cell expressions are tightly intertwined with a metabolic pathway in a colibactin-induced immune-suppressive microenvironment in RCC.

To further characterize the direct correlation between colibactin and lipid accumulation, we infected mouse colon cancer cell line (MC38) with CoPEC strain (11G5) or a mutant strain that does not produce colibactin (11G5ΔclbQ). Herein we show that the presence of CoPEC leads to lipid droplet accumulation (Figure 3G). We hypothesized that the accumulation of lipid droplets could be associated with the increase in PC by the *de-novo* pathway. Initially, we investigated the expression level of three lysophospholipid acyltransferases (LPCAT1,

LPCAT2 and LPCAT3), that converts lysophosphatidylcholine (LPC) into PC. Only LPCAT2 was highly expressed in MC38 cells (Figure 3H).

APC or KRAS mutation and loss of a c-type lectin cooperate to sustain a bacterial-induced glycerophospholipid in the tumor microenvironment from human RCC

To further define the differences of genes involved in the lipid metabolic pathway in both positive and negative CoPEC patients, we used the RNA sequencing (RNAseq) approach. By performing functional mapping and annotation (FUMA), we detected a low expression of genes with antimicrobial humoral immune response mediated by antimicrobial peptides including REG3A, REG1A, REG1B, F2, PF4V1, CXCL5, and DEFA6, particularly in patients with CMS3, colonized by positive CoPEC (Figures 4A and 4B). These patients that are characterized by the predominance of the APC mutation also showed enrichment in the lipid metabolic biological process (Figures 4C and 4D). In addition, these patients showed a low PDL1 expression and will potentially be resistant to immunotherapy (Figure 4E).

Herein, we found that REG3A, a gene that encodes a c-type lectin that demonstrates bactericidal activity, has a significant negative correlation with lipid metabolic pathway in patients with KRAS-mutant ($r=-0.89$ and $p=0.006$) and with APC-mutant ($r=-0.59$ and $p=0.01$) tumors. Interestingly, when analyzing wild-type KRAS and APC patients, there was no significant correlation (Figure 4F). It is important to note that regardless of the CMS, when we analyzed the differential gene expression including only patients colonized by positive COPEC, tumors with exacerbated glycerophospholipid intensity are associated with an increase of phosphoinositide-3-kinase (PIK3CD, PIK3R5 and PIK3R6) (Figure 4G). In contrast, limiting only patients who do not have colibactin, tumors with a high expression of glycerophospholipids and low REG3A expression display an increase of Ig such as IGSF23 (Figure 4H). Together, these data show that an altered lipid metabolic pathway is associated with transcriptional changes in human RCC.

Loss of a c-type lectin in mice enhances growth at the proximal colon of tumors with a microenvironment that impedes immune surveillance

Studies have shown that cancer-derived Ig acts as a crucial protumorigenic molecule that promotes carcinogenesis via several different mechanisms (14). As mentioned above, we found that patients with a high expression of glycerophospholipids are associated with a low expression of REG3A, ortholog of which is Reg3b in mice. To validate this finding, we examined intestinal tumorigenesis when subjecting Reg3b-deficient ($Reg3b^{-/-}$) mice and wild-

type controls to mutagen azoxymethane (AOM) followed by chronic exposure to dextran sodium sulfate (DSS) in the drinking water. DSS is a sulfated polysaccharide that is known to promote epithelial tissue disruption and microbial translocation (15). We demonstrate that, compared to wild animals, tumors of Reg3b$^{-/-}$ mice were closer to the proximal colon, reminiscent of the location of tumors in RCC patients (Figure 5A). Of importance, we noticed that Reg3b deficiency resulted in an alteration of the tumoral immune microenvironment, reflected by a decreased gene expression in M2-type macrophages genes markers (eg. Arg1 and Ccl24) coincided with a greater expression of several immunoglobulins heavy and light variable chains (Ighv1-58, Ighv1-62-3, Ighv1-71, Ighv1-72, Ighv1-74, Igkv13-85, Igkv8-19, Igkv8-26 and Igkv9-120) in tumor tissues (Figure 5B and 5C). Since Reg3b is thought to directly modulate host-microbiota, we next considered the possibility that loss of the biological activity of Reg3b may alter the tumor expression of Immunoglobuins in the presence of colibactin. This hypothesis led us to investigate protein expression levels in fecal lysate from mice infected or non with CoPEC strain. Interestingly, we observed that there was a decrease in IgA protein in CoPEC-infected Reg3b$^{-/-}$ mice compared to non-infected Reg3b$^{-/-}$ mice (Figure 5D).

DISCUSSION

Despite of high heterogeneity of CRC has become evident (16–18), it remains a prerequisite to defining how inter-tumor heterogeneity and differences between cancer cells within a tumor can lead to a variable response to therapies. In this context, bulk analysis obscured our understanding of how host-microbiota is locally regulated in solid tumors because this approach cannot provide insights into the molecular events that occurred sequentially or in parallel throughout the development of the tumor (4,19). Applying the state-of-the-art high-throughput *in situ* spatial profiling technologies, this study provides the first results compelling evidence that the metabolic heterogeneity driven by the bacteria microniches can create a potential vulnerability to immunotherapies, preferentially in patients colonized by positive CoPEC.

Intratumoral microbial components are closely associated with cancer initiation and development and affect anti-cancer approaches' therapeutic potential (20–23). Here, unbiased genomic analyses revealed an enrichment of the genus *Escherichia-Shigella* and the specie *Escherichia coli* increasing in relapse RCC patients and we showed that the colonization by CoPEC is an unfavorable prognostic factor in RCC. Consistent with this result, Bonnet et al. (24) reported a poor-prognosis outcome is related to the intra-tumoral CoPEC, which is

detected in about 50 to 60% of human colorectal cancer biopsies compared to ~20% of patients with diverticulosis (23,25). In relation to the different bacterial taxa, along with the *Escherichia-Shigella* group, nine bacterial ASVs linked to *Prevotella 9, four* different *Bacteroides* species *(B. uniformis, B. fragilis, B. stercoris, B. salyersiae), Lachnoclostridium, Barnesiella,* and *Odoribacter splanchnicus* were significantly increased in the positive CoPEC group. A majority of detected bacteria (6 out of 10) in this group were previously associated with the development of intestinal inflammation or CRC (26–28). Others such as *Fusobacterium, Acidaminococcus* and *Bacteroides vulgatus* were significantly depleted in the positive CoPEC patients. Only *Acidaminococcus* and *Bacteroides vulgatus* previously have been associated with a decrease in the number of patients with various inflammatory bowel disease conditions compared with controls (29). However, other bacteria identified in this group (such as *Megasphaera, Treponema denticola, Collinsella tanakaei, Fusobacterium, Fusobacterium mortiferum, Fusobacterium gonidiaformans*) provoke or participate in inflammatory processes or carcinogenesis (30,31). The decrease of these bacteria in the presence of positive CoPEC, nevertheless, indicates that the cellular and/or metabolic processes induced by bacteria can take place in different ways. Further studies focusing on microbiota modulation as a potential treatment for colibactin-associated RCC are therefore strongly encouraged.

Much effort has been spent to understand the mechanism of colibactin in human CRC. A recent study determined a specific DNA damage signature with an AT-rich hexameric sequence motif where colibactin-induced DSBs preferably occur termed as the colibactin damage motif (CDM), which exhibits an increased mutational load (32). Furthermore, was describe mutations at CDMs in CRC driver genes, such as APC (33). In this same sense, infection by CoPEC can promote colon tumorigenesis in APCMin/$^{+}$ mice (24,34). Our findings here are well in line with those observations. For instance, RCC patients colonized by positive CoPEC showed bearing mutations in either APC or KRAS and are classified into the CMS3. In agreement, this CMS subtype is defined by evident metabolic dysregulation and is significantly enriched by APC and KRAS mutations (35,36).

We further observed that cytotoxic CD8^{+} T cell proportion was distinct between positive and negative CoPEC patients, suggesting the heterogeneity of the immune microenvironment tumor. However, only applying *in situ* spatial analysis, we clarified that local bacteria microniches are characterized by a decrease of tumor-infiltrating CD8^{+} T cells, mainly in patients colonized by positive CoPEC. In support, Lopès et al. (10) showed a decrease of CD3^{+} and CD8^{+} T-cells with decreases in the anti-PD-1 immunotherapy efficacy in mice infected by

CoPEC. Likewise, a work focused on the effect spatial of the intratumoral microbiota in cancer, reported an increase in $CD11b^+$ and $CD66b^+$ myeloid cells but lower densities of $CD4^+$ and $CD8^+$ T cells in bacteria-positive microniches when compared to bacteria-negative areas.

The metabolomic bulk analysis is important to identify biomarkers and metabolic pathways altered in the cancer (5,37,38), but an insufficient approach to indicate the effect of the tumor-associated microbiota locally. Knowing this, applying a spatially resolved metabolomics approach, our study uncovered spatial metabolomic patterns that are present in bacteria microniches characterized by a unique lipid signature in patients colonized by CoPEC. In accordance with altered glycerophospholipids metabolism in different types of cancer including CRC (39–41), we also identified the spatial distribution discrepancy of PA, PC, PI, PE, PS, and PG in bacteria microniches between positive and negative CoPEC groups.

Alterations in phospholipid metabolism and, consequently, lipid composition has important therapeutic implications (42,43). Specifically, colon cancer cells were positively correlated with the expression of LPCAT2, a lipid droplet-localized enzyme supporting PC synthesis, and are more resistant to chemotherapy (40). In fact, the major phospholipids of the lipid droplet can be synthesized by the *de-novo* pathway (also known as the Kennedy pathway) and the Lands cycle (44), but the specific enzymes involved in its biosynthesis of colibactin-induced glycerophospholipid have remained obscure. Notably, we validated that CoPEC leads to lipid droplet accumulation in colon cancer cells. Then, we hypothesized that the altered PC composition in RCC patients was caused by the specific LPCAT overexpression. Here, we revealed that LPCAT2 was significantly up-regulated in MC38 cells. Further research is necessary to clarify more precisely the molecular mechanism that metabolic reprogramming by colibactin may condition the efficacy of CRC treatments.

Dissecting the effects of colibactin in RCC around metabolomics and transcriptomics approaches will enable us a precise comprehension of how this genotoxin drives carcinogenesis. Here, we provide evidence of REG3A activity against CoPEC. Surprisingly, in a subset of CMS3 patients, 72% of RCC tumors with low REG3A expression are colonized by positive CoPEC. It is noteworthy that different Reg3 lectins have distinct spectra of antimicrobial activity. In particular, Reg3b is involved not only Gram-positive bacteria but also some certain Gram-negative bacterial species, including different *Escherichia coli* strains (45). Probably, this antimicrobial peptide protects from bacterial genotoxin, which may be influenced by RCC-associated genetic alterations (KRAS or APC mutation). Another remarkable observation was the overexpression of Ig and the decrease of macrophages genes markers in the absence of Reg3b in mice. Interestingly, previous studies have demonstrated

that pathogen infection can regulate Ig expression in cancer cells and these Ig can promote protumorigenic effects via different mechanisms, mediating tumor immune escape (14,46). Moreover, Reg3b$^{-/-}$ mice infected with the CoPEC strain illustrated a decrease in the IgA protein in relation to Reg3b$^{-/-}$ mice non-infected. This suggests that Ig can actin as a switch between pro-tumoral and anti-tumoral Reg3b functionality.

In conclusion, our results using spatially-resolved metabolomic and transcriptomic approaches clarify how the presence of colibactin-producing bacteria may locally establish tumor heterogeneity for evading immune surveillance. These findings provide unique insights both for therapeutic intervention and enabling basic research into the mechanisms of microbiota-host interaction.

METHODS

Patient samples

All patients included in the analysis were diagnosed as sporadic cases and with tumors that arise in the cecum and ascending colon (right-sided colon). We used 77 samples of the Biobanks that have been set up at the Hospital Henri Mondor and at the Hospital of Clermont-Ferrand. A part of the patients was enrolled in several prospective cohorts named CCR1-3 (Acronyms Valihybritest and Vatnimad; for description, see Sobhani et al. (31) and on ClinicalTrials.gov: NCT01270360). This protocol has been approved by the ethics committee of *Comité de Protection des Personnes Paris Est-Henri Mondor* (no. 10-006 in 2010). Another part of these patients underwent surgery for CRC in the Digestive and Hepatobiliary Surgery Department of the University Hospital of Clermont–Ferrand. All patients were adult volunteers and signed informed consent before they were included in the study.

Identification of positive and negative CoPEC in the tumor tissue from RCC patients

We used two methods to validate the presence of pks island in the RCC tumor tissue. First, for patients from Hospital of Clermont-Ferrand, the samples were analyzed by PCR using specific primers located in the *clbB* and *clbN* genes of the pks island: *clbBr* (r for reverse orientation) (5′-CCA TTT CCC GTT TGA GCA CAC-3′), *clbBf* (f for forward orientation) (5′-GAT TTG GAT ACT GGC GAT AAC CG-3′), *clbNr* (5′-CAG TTC GGG TAT GTG TGG AAG G-3′), and *clbNf* (5′-GTT TTG CTC GCC AGA TAG TCA TTC-3′) (47).

Posteriorly, for all patients from this study, DNA extraction was performed from eight 50 µm cryosections of nitrogen frozen tissue using the QIAamp PowerFecal DNA Kit® (Qiagen, 12830-50) following the manufacturer's instructions with the following modification: 0.1 mm

diameter silica beads were added to the lysis solution provided and shaking was performed at maximum speed for 10 minutes in a vibratory shaker. DNA concentration was measured using the Qubit dsDNA Broad Range assay kit (Invitrogen Q32853). qPCR reactions were performed on a QuantStudioTM 7 Flex Real-Time PCR System (Applied Biosystems 4485701) in 384-well plates with 32ng of DNA, in a final volume of 8µl. Three technical replicates were performed for each sample. Primers and probes listed in the Table were used at a final concentration of 250nM.

Target	**Primers**	**Reference**
All bacteria 16S rDNA	F: 5'-CGGTGAATACGTTCCCGG-3' R: 5'-TACGGCTACCTTGTTACGACTT-3' Probe: 5' FAM-CTTGTACACACCGCCCGTC-TAM 3'	*Suzuki et al.* (48)
clbB	F: 5'-GCGCATCCTCAAGAGTAAATA-3' R: 5'-GCGCTCTATGCTCATCAACC-3' Probe: 5' FAM-TATTCGACACAGAACAACGCCGGT-TAM 3'	*Dejea et al.* (49)

The Master Mix Taqman (Applied Biosystems 4440038) was used with the following amplification steps: 50°C during 2min, 95°C during 15sec with 48 cycles, 60°C during 1min. The amount of *clbB* was determined using the QuantStudioTM Real-Time PCR software (version 1.7.2, Applied Biosystems) and the 2-ΔCt method, with all bacteria 16S rDNA as a calibrator. Patients with amplification were assigned as positive CoPEC.

Microbiota analysis

Total DNA from tumor tissue was used to perform microbiome analysis. Bacterial 16S rRNA gene V1-V2 region was amplified using 27F and 338R PCR primers and sequenced on a MiSeq (2×250 bp; Illumina, Hayward, CA). Bioinformatic processing and statistical analysis was performed in R software environment as described previously [1]. Briefly, paired-end fastq files without barcodes and adapters have been quality checked, denoised and prepared for further analysis using the dada2 package (50). Bacterial sequencies from amplicon sequence variant (ASV) table were annotated using latest silva database (version 138.1) (51). Data normalization and beta-diversity analysis were performed on each taxonomical level using DESeq2 package (52). To improve power of detecting differentially abundant taxa, only those bacteria that appeared in 25% of samples at least in one of the compared groups were used for

differential abundance analysis. Differences were considered significant when the corrected p-value (p adjusted) was < 0.05. Principal Coordinate Analysis (PCoA) with Bray-Curtis distances matrix based on Deseq2 normalized data was performed to visualize complex data and to get a new set of principal coordinates. Multivariate ANOVA based on similarity tests (Adonis) was performed with 9999 permutations of the data.

Tissue processing and FISH

Samples of RCC tumor tissue were collected within 30 minutes after surgical resection and immediately frozen in liquid nitrogen and stored at -80°C until further use. This analysis was conducted on 5 µm sections of 77 sporadic RCC patients' samples using cryostat at -21°C. Serial adjacent sections were obtained for fluorescence *in situ* hybridization (FISH) and hematoxylin and eosin (H&E) staining. Tissues were visualized by a pathologist to obtain tumor area and bacteria were stained by FISH using the general bacterial rRNA probe, EUB338 conjugated with Alexa 555 as described previously (53).

Spatial transcriptomic using RNAscope *in situ* hybridization

RNAscope multiplex fluorescent reagent 2.5 HD kit assay (Advanced cell diagnostics, Newark, CA, USA) was performed using frozen RCC tissue and cryostat cut sections of 10 µm were collected and mounted onto Superfrost™ Plus microscope slides. Slides were immersed in the 4% PFA for 1h at 4°C. Posteriorly, the sections were dehydrated and slides were baked for 1h at 60°C and a hydrophobic barrier was drawn around the tumor tissue. Endogenous peroxidases were blocked using a hydrogen peroxide solution for 10 min at room temperature and then, was used RNAscope proteas IV sob under the same conditions. The probes hybridization process was performed using the HybEZ™ II oven for 2h at 40°C for Hs-IFNy (310501, Opal 570), Hs-CD3E (553971-C2, Opal 650) and Hs-CD8A (560391-C3, Opal 520) probes. Between each amplification and staining step, slides were washed twice in 1X RNAscope wash buffer for two minutes. Then, the slides were incubated with DAPI (ThermoFisher Scientific) for 3 min at room temperature and placed with ProLong Gold antifade mounting solution (ThermoFisher Scientific) prior to imaging.

Spatial metabolomic using MALDI-FTICR imaging

This analysis was conducted on 10 µm sections of the 77 human RCC obtained in a cryostat at -21°C and mounted on ITO slides. On each slide, a quality control section (rat kidney homogenate spiked with Rutine) was added. Imaging of the tumors was performed at 80 µm

using a 7T-MALDI-FTICR in full scan mode (75 – 1000) and in negative ion mode. Following the acquisition, the MALDI matrix was removed in a bath of methanol and an H&E staining was performed. In particular, we conducted an *in situ* metabolites analysis dependent on the presence of bacteria in 12 sporadic RRC patients. Afterward, we identified positive and negative CoPEC patients. The normalized root-mean-square was applied and differential metabolite expression was determined using the *limma* package in R software. The following criteria were applied: p-value produced by Mann−Whitney−Wilcoxon test after FDR correction < 0.05, fold change > 1 or < -1). Volcano plot was used to present differential expressed metabolites with the EnhancedVolcano R package (version 4.0.3). Data acquisition, processing, and data visualization were performed using FlexImaging 4.1 and Multimaging 1.1 (ImaBiotech SAS, France). MSI data were acquired from each tissue section as well as matrix control areas adjacent to the tissue sections to check for analyte dispersion during sample preparation. Metabolite annotation was performed according to Lipid maps (http://www.lipidmaps.org/) and Metlin (https://metlin.scripps.edu).

RNA extraction, RNA sequencing and qRT-PCR

Total RNA was extracted by using the column-based RNeasy Mini Kit and RNeasy Micro Kit according to the manufacturer's instructions (Qiagen). Complementary DNA was generated by using the AffinityScript QPCR cDNA Synthesis Kit and analysis of gene expression was performed on StratageneTM Mx3005P by using the Brillant III Ultra-Fast SYBR® Green QPCR Master Mix (all Agilent Technologies).

Cell culture, bacterial infection and lipid droplets

The MC38 cell line, derived from methylcholanthrene-induced C57BL6 murine colon adenocarcinoma cells was maintained in DMEM supplemented with 10% FBS, 1mM L-Glutamine, and Penicillin (100 µ/ml) – Streptomycin (0.1 mg/ml), at 37 °C under 5% CO2 pressure. Cells were routinely tested for mycoplasma. All media components were obtained from Sigma-Aldrich. Treatments were carried out using the clinical CoPEC 11G5 strain isolated from a patient with CRC and its isogenic mutant 11G5ΔclbQ, depleted for the clbQ gene in the pks island and unable to produce colibactin. These strains were grown at 37 °C in Luria-Bertani medium overnight. For bacterial infections, cells were infected at a multiplicity of infection (MOI) of 100 bacteria for 3 h and cells remained in culture for 5 days after infection. Cells were washed three times with PBS and DMEM with 100 µg/mL gentamicin was added (34).

Lipid droplets were analyzed using Nile red (Molecular Probes) at 1:2000 in PBS for 15 min and then fixed in 4% PFA for 10 min at 4 °C. The slides were mounted in ProLong Gold Antifade with DAPI (Molecular Probes) before imaging. Images were acquired with an Axio Imager M2 (Zeiss) coupled with an Apotome.2 (×63 objective).

Colitis-associated cancer in animals

Reg3b$^{-/-}$ or Reg3b$^{+/+}$ mice were given 2.5 and 3% (w/v) DSS in drinking water ad libitum by changing DSS solution every three days. Analysis of recovery of DSS-induced colitis was performed by replacing DSS solution by drinking water. Susceptibility to DSS-induced colitis and recovery were assessed daily by monitoring body weight loss and disease activity index according to the scoring scheme as described previously (54). As a model of colitis-associated cancer, mice were i.p. injected with azoxymethane (AOM) in a concentration of 8 mg/kg 5 days prior to DSS administration. 2% (w/v) DSS was given in drinking water ad libitum for 7 days followed by 10 days of water administration. DSS/water treatment was repeated four times and tumor growth was monitored by video colonoscopy on day 10 of each water cycle.

Identification of IgA after bacterial infection in mice

Infection in Reg3b$^{-/-}$ or Reg3b$^{+/+}$ mice was conducted as described previously (10). In brief, to enhance *Escherichia coli* strain colonization, we administered streptomycin (2.5 g/l) for 3 days prior to oral inoculation with bacteria ($\approx 1 \times 10^8$ bacteria in PBS) or PBS (non-infected group). For measurement of commensal bacteria-specific IgA, fecal bacteria were isolated from mice used to coat ELISA plates. Fecal bacteria from ~100 mg fecal pellets were isolated by homogenization in sterile PBS and separated from debris/mouse cells by removing the pellet after centrifugation at 1,000 rpm for 5 min. Isolated fecal bacteria were washed twice, heat-killed at 85° C for 1 hr, and resuspended in 10 ml coating buffer, and 100 μL was added to each well of a 96-well ELISA plate for overnight coating at 4° C. Wells were blocked with 1% (w/v) BSA in PBS for 2 hr at room temperature. Mouse sera were diluted at 1:100 and incubated overnight at 4° C for detection of IgA.

Statistical Analysis

Progression-free survival (PFS) was evaluated using Kaplan–Meier method available in the R (version 4.0.3) package survival. The p values are from log-rank tests. Statistical analysis was performed using GraphPad Prism version 6.0 (GraphPad Software). Significant differences were considered: ns (nonsignificant difference); *, $p < 0.05$; **, $p < 0.01$; ***, $p < 0.001$ by

multiple comparison tests (one-way ANOVA or Kruskal–Wallis depending on data distribution) followed by post hoc tests (Bonferroni multiple comparisons tests), as detailed in the figure legends.

Acknowledgments

Funding support for this research was provided by the following grants: BpiFrance, Fondation i-SITE, Fondation pour la Recherche Médicale, Inserm - Grand Programme Transversal Microbiote, ITMO Cancer AVIESAN, Plan Cancer (HTE201601) and Région Hauts-de-France. We would like to thank the BioImaging Center Lille platform for assistance with image acquisition.

Declaration of interests

The authors declare no competing interests regarding these data and materials.

REFERENCES

1. WHO. Cancer [Internet]. [cited 2022 Oct 5]. Available from: https://www.who.int/news-room/fact-sheets/detail/cancer
2. Baran B, Mert Ozupek N, Yerli Tetik N, Acar E, Bekcioglu O, Baskin Y. Difference Between Left-Sided and Right-Sided Colorectal Cancer: A Focused Review of Literature. Gastroenterol Res [Internet]. 2018;11:264–73. Available from: http://www.gastrores.org/index.php/Gastrores/article/view/1062
3. Sagaert X, Vanstapel A, Verbeek S. Tumor Heterogeneity in Colorectal Cancer: What Do We Know So Far? Pathobiology [Internet]. 2018;85:72–84. Available from: https://www.karger.com/Article/FullText/486721
4. Galeano Niño JL, Wu H, LaCourse KD, Kempchinsky AG, Baryiames A, Barber B, et al. Effect of the intratumoral microbiota on spatial and cellular heterogeneity in cancer. Nature [Internet]. 2022;611:810–7. Available from: https://www.nature.com/articles/s41586-022-05435-0
5. Snaebjornsson MT, Janaki-Raman S, Schulze A. Greasing the Wheels of the Cancer Machine: The Role of Lipid Metabolism in Cancer. Cell Metab [Internet]. 2020;31:62–76. Available from: https://linkinghub.elsevier.com/retrieve/pii/S1550413119306175
6. Zhao S-S, Chen L, Yang J, Wu Z-H, Wang X-Y, Zhang Q, et al. Altered Gut Microbial Profile Accompanied by Abnormal Fatty Acid Metabolism Activity Exacerbates

Endometrial Cancer Progression. Zhang L, editor. Microbiol Spectr [Internet]. 2022;10. Available from: https://journals.asm.org/doi/10.1128/spectrum.02612-22

7. Dalmasso G, Cougnoux A, Delmas J, Darfeuille-Michaud A, Bonnet R. The bacterial genotoxin colibactin promotes colon tumor growth by modifying the tumor microenvironment. Gut Microbes [Internet]. 2014;5:675–80. Available from: http://www.tandfonline.com/doi/full/10.4161/19490976.2014.969989

8. Nougayrède J-P, Homburg S, Taieb F, Boury M, Brzuszkiewicz E, Gottschalk G, et al. Escherichia coli Induces DNA Double-Strand Breaks in Eukaryotic Cells. Science (80-) [Internet]. 2006;313:848–51. Available from: https://www.science.org/doi/10.1126/science.1127059

9. Wilson MR, Jiang Y, Villalta PW, Stornetta A, Boudreau PD, Carrá A, et al. The human gut bacterial genotoxin colibactin alkylates DNA. Science (80-) [Internet]. 2019;363. Available from: https://www.science.org/doi/10.1126/science.aar7785

10. Lopès A, Billard E, Casse AH, Villéger R, Veziant J, Roche G, et al. Colibactin-positive <scp> *Escherichia coli* </scp> induce a procarcinogenic immune environment leading to immunotherapy resistance in colorectal cancer. Int J Cancer [Internet]. 2020;146:3147–59. Available from: https://onlinelibrary.wiley.com/doi/10.1002/ijc.32920

11. Wang L, Quan Y, Zhu Y, Xie X, Wang Z, Wang L, et al. The regenerating protein 3A: a crucial molecular with dual roles in cancer. Mol Biol Rep [Internet]. 2022;49:1491–500. Available from: https://link.springer.com/10.1007/s11033-021-06904-x

12. Rao A, Barkley D, França GS, Yanai I. Exploring tissue architecture using spatial transcriptomics. Nature [Internet]. 2021;596:211–20. Available from: https://www.nature.com/articles/s41586-021-03634-9

13. Wang F, Flanagan J, Su N, Wang L-C, Bui S, Nielson A, et al. RNAscope. J Mol Diagnostics [Internet]. 2012;14:22–9. Available from: https://linkinghub.elsevier.com/retrieve/pii/S1525157811002571

14. Cui M, Huang J, Zhang S, Liu Q, Liao Q, Qiu X. Immunoglobulin Expression in Cancer Cells and Its Critical Roles in Tumorigenesis. Front Immunol [Internet]. 2021;12. Available from: https://www.frontiersin.org/articles/10.3389/fimmu.2021.613530/full

15. Strober W, Fuss IJ, Blumberg RS. The Immunology of Mucosal Models of Inflammation. Annu Rev Immunol [Internet]. 2002;20:495–549. Available from: https://www.annualreviews.org/doi/10.1146/annurev.immunol.20.100301.064816

16. Molinari C, Marisi G, Passardi A, Matteucci L, De Maio G, Ulivi P. Heterogeneity in

Colorectal Cancer: A Challenge for Personalized Medicine? Int J Mol Sci [Internet]. 2018;19:3733. Available from: http://www.mdpi.com/1422-0067/19/12/3733

17. Zheng Z, Yu T, Zhao X, Gao X, Zhao Y, Liu G. Intratumor heterogeneity: A new perspective on colorectal cancer research. Cancer Med [Internet]. 2020;9:7637–45. Available from: https://onlinelibrary.wiley.com/doi/10.1002/cam4.3323

18. Buikhuisen JY, Torang A, Medema JP. Exploring and modelling colon cancer inter-tumour heterogeneity: opportunities and challenges. Oncogenesis [Internet]. 2020;9:66. Available from: https://www.nature.com/articles/s41389-020-00250-6

19. Gilson P, Merlin J-L, Harlé A. Deciphering Tumour Heterogeneity: From Tissue to Liquid Biopsy. Cancers (Basel) [Internet]. 2022;14:1384. Available from: https://www.mdpi.com/2072-6694/14/6/1384

20. Sadrekarimi H, Gardanova ZR, Bakhshesh M, Ebrahimzadeh F, Yaseri AF, Thangavelu L, et al. Emerging role of human microbiome in cancer development and response to therapy: special focus on intestinal microflora. J Transl Med [Internet]. 2022;20:301. Available from: https://translational-medicine.biomedcentral.com/articles/10.1186/s12967-022-03492-7

21. Yang L, Li A, Wang Y, Zhang Y. Intratumoral microbiota: roles in cancer initiation, development and therapeutic efficacy. Signal Transduct Target Ther [Internet]. 2023;8:35. Available from: https://www.nature.com/articles/s41392-022-01304-4

22. Sepich-Poore GD, Zitvogel L, Straussman R, Hasty J, Wargo JA, Knight R. The microbiome and human cancer. Science (80-) [Internet]. 2021;371. Available from: https://www.science.org/doi/10.1126/science.abc4552

23. Arthur JC, Perez-Chanona E, Mühlbauer M, Tomkovich S, Uronis JM, Fan T-J, et al. Intestinal Inflammation Targets Cancer-Inducing Activity of the Microbiota. Science (80-) [Internet]. 2012;338:120–3. Available from: https://www.science.org/doi/10.1126/science.1224820

24. Bonnet M, Buc E, Sauvanet P, Darcha C, Dubois D, Pereira B, et al. Colonization of the Human Gut by E. coli and Colorectal Cancer Risk. Clin Cancer Res [Internet]. 2014;20:859–67. Available from: https://aacrjournals.org/clincancerres/article/20/4/859/78872/Colonization-of-the-Human-Gut-by-E-coli-and

25. Buc E, Dubois D, Sauvanet P, Raisch J, Delmas J, Darfeuille-Michaud A, et al. High Prevalence of Mucosa-Associated E. coli Producing Cyclomodulin and Genotoxin in Colon Cancer. Battista JR, editor. PLoS One [Internet]. 2013;8:e56964. Available from:

https://dx.plos.org/10.1371/journal.pone.0056964

26. Snezhkina A V., Krasnov GS, Lipatova A V., Sadritdinova AF, Kardymon OL, Fedorova MS, et al. The Dysregulation of Polyamine Metabolism in Colorectal Cancer Is Associated with Overexpression of c-Myc and C/EBP β rather than Enterotoxigenic Bacteroides fragilis Infection. Oxid Med Cell Longev [Internet]. 2016;2016:1–11. Available from: http://www.hindawi.com/journals/omcl/2016/2353560/

27. Lv Y, Ye T, Wang H-P, Zhao J-Y, Chen W-J, Wang X, et al. Suppression of colorectal tumorigenesis by recombinant Bacteroides fragilis enterotoxin-2 in vivo. World J Gastroenterol [Internet]. 2017;23:603. Available from: http://www.wjgnet.com/1007-9327/full/v23/i4/603.htm

28. Lucas C, Barnich N, Nguyen H. Microbiota, Inflammation and Colorectal Cancer. Int J Mol Sci [Internet]. 2017;18:1310. Available from: https://www.mdpi.com/1422-0067/18/6/1310

29. Lin C, Li B, Tu C, Chen X, Guo M. Correlations between Intestinal Microbiota and Clinical Characteristics in Colorectal Adenoma/Carcinoma. Liao Z, editor. Biomed Res Int [Internet]. 2022;2022:1–11. Available from: https://www.hindawi.com/journals/bmri/2022/3140070/

30. Bullman S, Pedamallu CS, Sicinska E, Clancy TE, Zhang X, Cai D, et al. Analysis of Fusobacterium persistence and antibiotic response in colorectal cancer. Science (80-) [Internet]. 2017;358:1443–8. Available from: https://www.science.org/doi/10.1126/science.aal5240

31. Sobhani I, Bergsten E, Couffin S, Amiot A, Nebbad B, Barau C, et al. Colorectal cancer-associated microbiota contributes to oncogenic epigenetic signatures. Proc Natl Acad Sci [Internet]. 2019;116:24285–95. Available from: https://pnas.org/doi/full/10.1073/pnas.1912129116

32. Dziubańska-Kusibab PJ, Berger H, Battistini F, Bouwman BAM, Iftekhar A, Katainen R, et al. Colibactin DNA-damage signature indicates mutational impact in colorectal cancer. Nat Med [Internet]. 2020;26:1063–9. Available from: https://www.nature.com/articles/s41591-020-0908-2

33. Pleguezuelos-Manzano C, Puschhof J, Rosendahl Huber A, van Hoeck A, Wood HM, Nomburg J, et al. Mutational signature in colorectal cancer caused by genotoxic pks+ E. coli. Nature [Internet]. 2020;580:269–73. Available from: https://www.nature.com/articles/s41586-020-2080-8

34. Lucas C, Salesse L, Hoang MHT, Bonnet M, Sauvanet P, Larabi A, et al. Autophagy of

Intestinal Epithelial Cells Inhibits Colorectal Carcinogenesis Induced by Colibactin-Producing Escherichia coli in Apc Mice. Gastroenterology [Internet]. 2020;158:1373–88. Available from: https://linkinghub.elsevier.com/retrieve/pii/S0016508520300068

35. Guinney J, Dienstmann R, Wang X, de Reyniès A, Schlicker A, Soneson C, et al. The consensus molecular subtypes of colorectal cancer. Nat Med [Internet]. 2015;21:1350–6. Available from: http://www.nature.com/articles/nm.3967

36. Inamura K. Colorectal Cancers: An Update on Their Molecular Pathology. Cancers (Basel) [Internet]. 2018;10:26. Available from: https://www.mdpi.com/2072-6694/10/1/26

37. Pavlova NN, Zhu J, Thompson CB. The hallmarks of cancer metabolism: Still emerging. Cell Metab [Internet]. 2022;34:355–77. Available from: https://linkinghub.elsevier.com/retrieve/pii/S1550413122000225

38. Vasseur S, Guillaumond F. Lipids in cancer: a global view of the contribution of lipid pathways to metastatic formation and treatment resistance. Oncogenesis [Internet]. 2022;11:46. Available from: https://www.nature.com/articles/s41389-022-00420-8

39. Morita Y, Sakaguchi T, Ikegami K, Goto-Inoue N, Hayasaka T, Hang VT, et al. Lysophosphatidylcholine acyltransferase 1 altered phospholipid composition and regulated hepatoma progression. J Hepatol [Internet]. 2013;59:292–9. Available from: https://linkinghub.elsevier.com/retrieve/pii/S0168827813002110

40. Cotte AK, Aires V, Fredon M, Limagne E, Derangère V, Thibaudin M, et al. Lysophosphatidylcholine acyltransferase 2-mediated lipid droplet production supports colorectal cancer chemoresistance. Nat Commun [Internet]. 2018;9:322. Available from: http://www.nature.com/articles/s41467-017-02732-5

41. Uehara T, Kikuchi H, Miyazaki S, Iino I, Setoguchi T, Hiramatsu Y, et al. Overexpression of Lysophosphatidylcholine Acyltransferase 1 and Concomitant Lipid Alterations in Gastric Cancer. Ann Surg Oncol [Internet]. 2016;23:206–13. Available from: http://link.springer.com/10.1245/s10434-015-4459-6

42. Stoica C, Ferreira AK, Hannan K, Bakovic M. Bilayer Forming Phospholipids as Targets for Cancer Therapy. Int J Mol Sci [Internet]. 2022;23:5266. Available from: https://www.mdpi.com/1422-0067/23/9/5266

43. Munir R, Lisec J, Swinnen J V., Zaidi N. Lipid metabolism in cancer cells under metabolic stress. Br J Cancer [Internet]. 2019;120:1090–8. Available from: http://www.nature.com/articles/s41416-019-0451-4

44. Moessinger C, Klizaite K, Steinhagen A, Philippou-Massier J, Shevchenko A, Hoch M,

et al. Two different pathways of phosphatidylcholine synthesis, the Kennedy Pathway and the Lands Cycle, differentially regulate cellular triacylglycerol storage. BMC Cell Biol [Internet]. 2014;15:43. Available from: https://bmcmolcellbiol.biomedcentral.com/articles/10.1186/s12860-014-0043-3

45. Miki T, Holst O, Hardt W-D. The Bactericidal Activity of the C-type Lectin RegIIIβ against Gram-negative Bacteria involves Binding to Lipid A. J Biol Chem [Internet]. 2012;287:34844–55. Available from: https://linkinghub.elsevier.com/retrieve/pii/S0021925820628137

46. Hu F, Zhang L, Zheng J, Zhao L, Huang J, Shao W, et al. Spontaneous Production of Immunoglobulin M in Human Epithelial Cancer Cells. Fuxe J, editor. PLoS One [Internet]. 2012;7:e51423. Available from: https://dx.plos.org/10.1371/journal.pone.0051423

47. Johnson JR, Johnston B, Kuskowski MA, Nougayrede J-P, Oswald E. Molecular Epidemiology and Phylogenetic Distribution of the Escherichia coli pks Genomic Island. J Clin Microbiol [Internet]. 2008;46:3906–11. Available from: https://journals.asm.org/doi/10.1128/JCM.00949-08

48. Suzuki MT, Taylor LT, DeLong EF. Quantitative Analysis of Small-Subunit rRNA Genes in Mixed Microbial Populations via 5′-Nuclease Assays. Appl Environ Microbiol [Internet]. 2000;66:4605–14. Available from: https://journals.asm.org/doi/10.1128/AEM.66.11.4605-4614.2000

49. Dejea CM, Fathi P, Craig JM, Boleij A, Taddese R, Geis AL, et al. Patients with familial adenomatous polyposis harbor colonic biofilms containing tumorigenic bacteria. Science (80-) [Internet]. 2018;359:592–7. Available from: https://www.science.org/doi/10.1126/science.aah3648

50. Callahan BJ, McMurdie PJ, Rosen MJ, Han AW, Johnson AJA, Holmes SP. DADA2: High-resolution sample inference from Illumina amplicon data. Nat Methods [Internet]. 2016;13:581–3. Available from: http://www.nature.com/articles/nmeth.3869

51. Quast C, Pruesse E, Yilmaz P, Gerken J, Schweer T, Yarza P, et al. The SILVA ribosomal RNA gene database project: improved data processing and web-based tools. Nucleic Acids Res [Internet]. 2012;41:D590–6. Available from: http://academic.oup.com/nar/article/41/D1/D590/1069277/The-SILVA-ribosomal-RNA-gene-database-project

52. Love MI, Huber W, Anders S. Moderated estimation of fold change and dispersion for RNA-seq data with DESeq2. Genome Biol [Internet]. 2014;15:550. Available from:

http://genomebiology.biomedcentral.com/articles/10.1186/s13059-014-0550-8

53. Johansson ME V., Gustafsson JK, Sjöberg KE, Petersson J, Holm L, Sjövall H, et al. Bacteria Penetrate the Inner Mucus Layer before Inflammation in the Dextran Sulfate Colitis Model. Ernberg IT, editor. PLoS One [Internet]. 2010;5:e12238. Available from: https://dx.plos.org/10.1371/journal.pone.0012238

54. Rath E, Berger E, Messlik A, Nunes T, Liu B, Kim SC, et al. Induction of dsRNA-activated protein kinase links mitochondrial unfolded protein response to the pathogenesis of intestinal inflammation. Gut [Internet]. 2012;61:1269–78. Available from: https://gut.bmj.com/lookup/doi/10.1136/gutjnl-2011-300767

FIGURES

Figure 1. Right-sided colon cancer (RCC) patients differ in relation to bacteria composition and showed a poor progression free-survival with a predominance of metabolic CMS3 and APC mutation in patients colonized by colibactin. Principal Coordinate Analysis (PCoA) with Bray-Curtis distances matrix based on Deseq2 normalized data between healthy and relapse RCC patients: (A) Genus and (B) Species. The relative abundance between healthy and relapse RCC patients: (C) Genus and (D) Species. (E) Kaplan-Meier analysis showed that RCC patients colonized by positive colibactin-producing *Escherichia coli* (CoPEC) predict poor progression-free survival (p=0.018). (F) Bar graph showing the percentage of patients with the APC mutation in the negative and positive CoPEC groups in relation to consensus molecular subtypes (CMS). (G) Beta-diversity analysis results between positive and negative CoPEC patients. The left plot represents the $\log_2$ fold change value of the mean normalized abundance ratio of positive CoPEC vs. negative CoPEC; the middle plot represents the adjusted p-value obtained by Deseq2 differential abundance analysis; the right plot represents the mean normalized abundance for each significant abundance bacteria.

Figure 2. Spatial *in situ* analysis revealed an immunosuppressive effect of the tumor-associated bacterial microniches mainly in patients colonized by positive colibactin-producing *Escherichia coli* (CoPEC). (A) Representative image of RCC tumor showing bacteria stained with general rRNA probe EUB338 conjugated to Alexa 555 (orange) and the nuclear DNA stained with DAPI (blue) using *in situ* hybridization (FISH). (B) Violin plots showing the difference in the cytotoxic $CD8^+$ T cells proportion from positive and negative CoPEC patients using quanTIseq and EPIC analysis. (C) Representative images of H&E, FISH and RNAscope ($CD8^+$ T cells) from RRC tumors colonized by positive and negative CoPEC. White square: ROI without bacteria and orange square: ROI with bacteria. (D) Violin plots show $CD8^+$ spots quantification detected by the RNAscope in RRC patients colonized by positive and negative CoPEC.

Figure 3. Bacterial microniches revealed an increase in glycerophospholipid in colibactin-associated tumors. (A) Representative images of MALDI-based metabolomics combined FISH analysis (bacteria stained with general rRNA probe EUB338) from RCC patients colonized by positive and negative colibactin-producing *Escherichia coli* (CoPEC). White

square: ROI without bacteria and orange square: ROI with bacteria. (B and C) Volcano plot displaying metabolomic analysis from positive (ROI with bacteria versus ROI without bacteria) and negative CoPEC (ROI with bacteria versus ROI without bacteria) patients, respectively. Root means square normalization was applied, adjusted p. value (FDR correction) < 0.05, and logFC > 1 or < -1 were considered. (D) Heatmap showing differentially expressed lipids between negative and positive CoPEC groups. (E and F) Pearson correlation between $CD8^+$ spots detected by the RNAscope and phosphatidylcholine (PC) identified by the MALDI-FTICR in RRC patients colonized by positive and negative CoPEC, respectively. (G) Representative images of MC38 cells with Nile red staining and DAPI (×63 magnification) under different bacterial infections: CoPEC 11G5 strain (positive CoPEC), isogenic mutant 11G5ΔclbQ strain (negative CoPEC) and negative control (NC, non-infected). (H) Bar graph showing that CoPEC 11G5 strain (positive CoPEC) promotes an increase of LPCAT2 gene expression in MC38 cells.

Figure 4. The loss of a c-type lectin cooperates to sustain a bacterial-induced glycerophospholipid in the RCC tumors. (A) Volcano plot representation of gene differential expression from positive and negative colibactin-producing Escherichia coli (CoPEC) patients. (B) Gene expression heatmap of GO antimicrobial humoral immune response mediated by the antimicrobial peptide. CMS, CoPEC, REG3A expression status, APC and KRAS mutations status are added on left as color bars.

Significantly enriched gene-sets from the Gene Ontology (GO) - Biological Process category of the 128 up (C) - and 126 down (D)-regulated genes expression for RCC patients colonized by CoPEC. The blue bars represent the enrichment p-value (-log10 adjusted) after FDR correction considering the number of gene sets tested per category. The red bars indicate the proportion of overlapping inputted genes according to the size (number of genes) of each gene set. The orange squares show the inputted genes that are part of the enriched gene sets.

(E) Spearman correlation between REG3A gene expression and PDL1. (F) Spearman correlation between Reg3A gene expression and glycerophospholipid in groups with or without APC and KRAS mutation. (G) Volcano plot representation of differential gene expression from high and low glycerophospholipid intensity in positive CoPEC patients. (H) Volcano plot representation of differential gene expression from high and low glycerophospholipid intensity in negative CoPEC patients.

Figure 5. Reg3b-deficient mice enhance growth at the proximal colon of tumors with an increase of immunoglobulins. (A) Tumor counts by centimeter from right to left in colon *p<0.05 by pair-wise Mann-Whitney U test comparing corresponding colon centimeter sections. Box limits are set at the third and first quartile range with the central line at the median. Representative images below plots are examples of colon tumors from Reg3b-deficient (Reg3b$^{-/-}$) and wild-type mice (Reg3b$^{+/+}$) mice. (B) Heatmap showing the differential gene expression between Reg3b$^{-/-}$ versus Reg3b$^{+/+}$ in colon tumor. Immunoglobulins were clearly increased in Reg3b$^{-/-}$ colon tumors. (C) Color circles showing gene expression similarities between mice and human colon tumors. (D) Graph representing IgA protein expression of fecal samples from Reg3b$^{-/-}$ and Reg3b$^{-/-}$mice, infected or non-infected with CoPEC strain.

Supplementary

Figure S1. **Beta-diversity analysis results of CMS3 group between positive and negative patients colonized by colibactin-producing *Escherichia coli* (CoPEC)**. The left plot represents the $\log_2$ fold change value of the mean normalized abundance ratio of positive and negative CoPEC groups; the middle plot represents the p-value obtained by deseq2 differential abundance analysis; the right plot represents the mean normalized abundance for each significant abundance bacteria.

Figure S2. **Potential metabolomic biomarkers in right-sided colon cancer (RCC)**. Graphic showing the intensity of four metabolites (kinetin riboside, N-acetylneuraminic acid, piperidine and phosphatidic acid) differentially expressed between tumor and adjacent normal tissue using a high spectral resolution of the FTICR-MS.

Figure S3. Intratumoral microbiota has a heterogeneous distribution of metabolites in RCC tumor tissues. Venn diagram showing differentially expressed metabolites between negative and positive CoPEC groups and heatmap showing 11 specific metabolites from patients colonized by positive CoPEC.

A
Genus
Axis.2 [15.8%]
Axis.1 [18.9%]
Outcome healthy relapse
B
Species
Axis.2 [12.4%]
Axis.1 [19.8%]
Outcome healthy relapse
C
Genus
Relative abundance (%)
healthy
relapse
g__Bacteroides
g__Faecalibacterium
g__Prevotella 9
g__Fusobacterium
g__Escherichia-Shigella
g__Roseburia
g__Blautia
g__Selenomonas
g__Parabacteroides
g__Streptococcus
Others
D
Species
Relative abundance (%)
healthy
relapse
s__Escherichia-coli
s__unc. bacterium adhufec61-25
s__unc. Firmicutes bacterium
s__unc. bacterium adhufec55
s__Ruminococcus gnavus CC55-001C
s__Bacteroides plebeius DSM-17135
s__unc. Clostridium sp.
s__Campylobacter showae
s__Streptococcus gallolyticus subsppasteurianus
s__Streptococcus salivarius subspsalivarius
Others
E.
CoPEC
Stage
Sex
RCC
Presence of colibactin producing by E. coli (CoPEC)
Negative
Positive
Progression-free survival probability
p = 0.018
Duration in months
CoPEC
Positive
Negative
Stage
2
3
4
1
Sex
Woman
Man
F
CMS1
CMS2
CMS3
CMS4
Percentage
APC_mutation
No
Not analyzed
Yes
Negative
Positive
CoPEC
G
Phylum
Class
Order
Genus
Species
ASV
Synergistota
Synergistia
Synergistales
Actinomycetales
Megasphaera
Acidaminococcus
Prevotella 7
Treponema denticola
Collinsella tanakaei
Fusobacterium mortiferum
Escherichia-Shigella coli
Fusobacterium [ASV 24]
Fusobacterium mortiferum [ASV 143]
Fusobacterium gonidiaformans [ASV 487]
Prevotella 9 [ASV 51]
Prevotella intermedia [ASV 87]
Prevotella 9 [ASV 121]
Prevotella 7 [ASV 324]
Bacteroides massiliensis [ASV 63]
Bacteroides massiliensis [ASV 66]
Bacteroides uniformis [ASV 100]
Bacteroides fragilis [ASV 142]
Bacteroides stercoris [ASV 145]
Bacteroides plebeius [ASV 189]
Bacteroides uniformis [ASV 225]
Bacteroides vulgatus [ASV 289]
Bacteroides salyersiae [ASV 482]
Lachnoclostridium [ASV 459]
Lachnoclostridium [ASV 699]
Selenomonas sputigena [ASV 89]
Selenomonas sputigena [ASV 111]
Barnesiella [ASV 369]
Ruminococcus gnavus group [ASV 455]
Odoribacter splanchnicus [ASV 550]
UCG 2 [ASV 673]
log2FoldChange
p.adj (-Log10)
deseq2 normalized abundance
Phylum
Actinobacteriota
Bacteroidota
Firmicutes
Fusobacteriota
Proteobacteria
Synergistota
Spirochaetota
CoPEC
Negative
Positive

A.

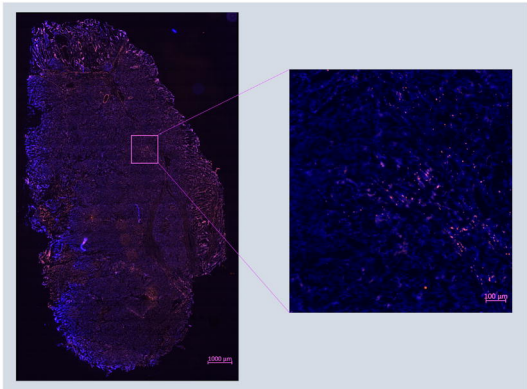
1000 µm
100 µm

B.

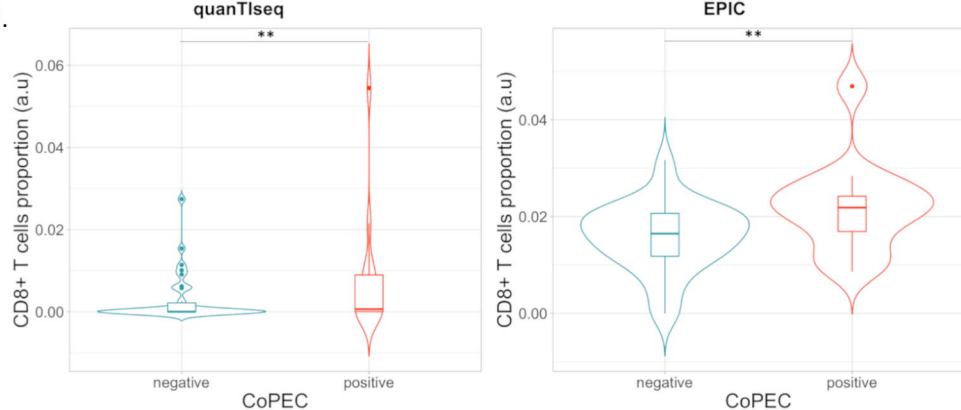
quanTIseq
EPIC
**
**
CD8+ T cells proportion (a.u)
0.06
0.04
0.02
0.00
negative
positive
CoPEC

C.

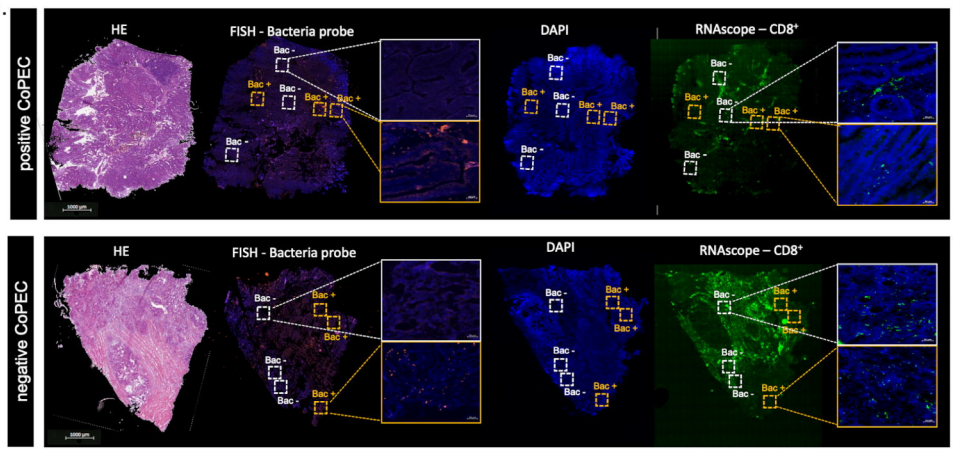
positive CoPEC
negative CoPEC
HE
FISH - Bacteria probe
DAPI
RNAscope – CD8+
Bac -
Bac +

D.

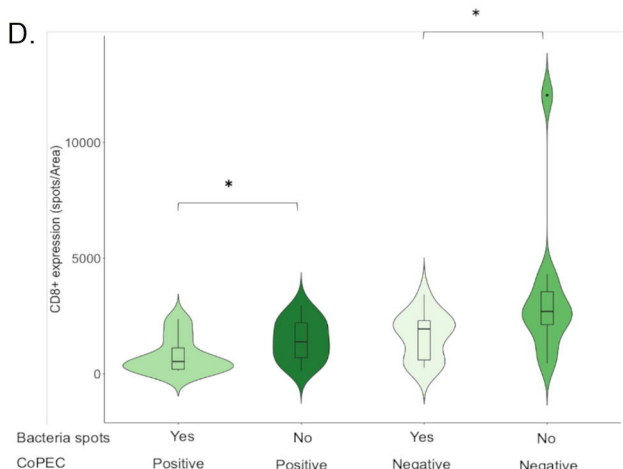
*
*
CD8+ expression (spots/Area)
10000
5000
0
Bacteria spots
CoPEC
Yes
Positive
No
Positive
Yes
Negative
No
Negative

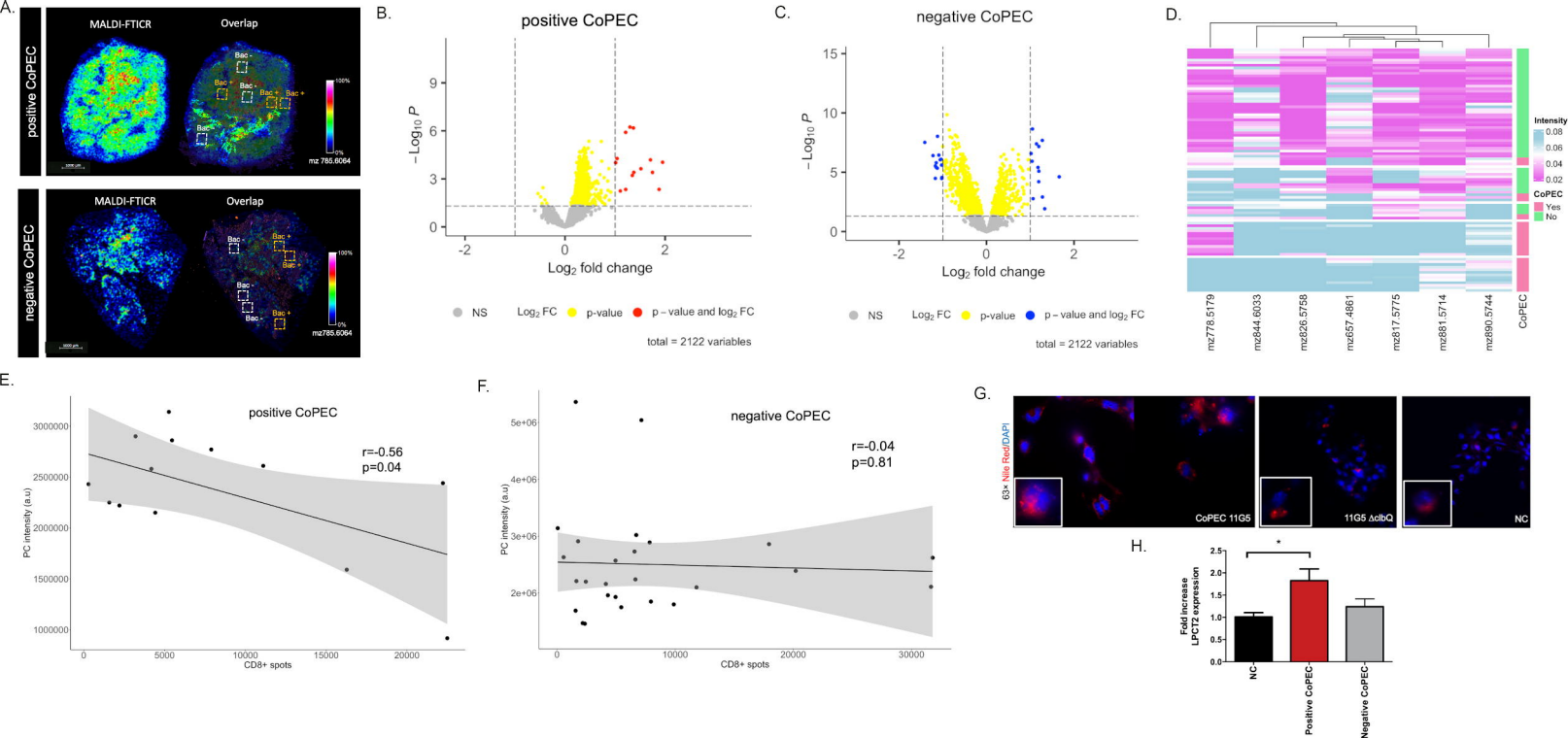
A.
positive CoPEC
MALDI-FTICR
Overlap
Bac -
Bac +
100%
0%
mz 785.6064
negative CoPEC
B.
positive CoPEC
$-Log_{10}$ P
Log_2 fold change
NS
Log_2 FC
p-value
p – value and log_2 FC
total = 2122 variables
C.
negative CoPEC
D.
Intensity
0.08
0.06
0.04
0.02
CoPEC
Yes
No
mz778.5179
mz844.6033
mz826.5758
mz657.4861
mz817.5775
mz881.5714
mz890.5744
E.
positive CoPEC
r=-0.56
p=0.04
PC intensity (a.u)
CD8+ spots
F.
negative CoPEC
r=-0.04
p=0.81
G.
63x Nile Red/DAPI
CoPEC 11G5
11G5 ΔclbQ
NC
H.
Fold Increase LPCT2 expression
NC
Positive CoPEC
Negative CoPEC

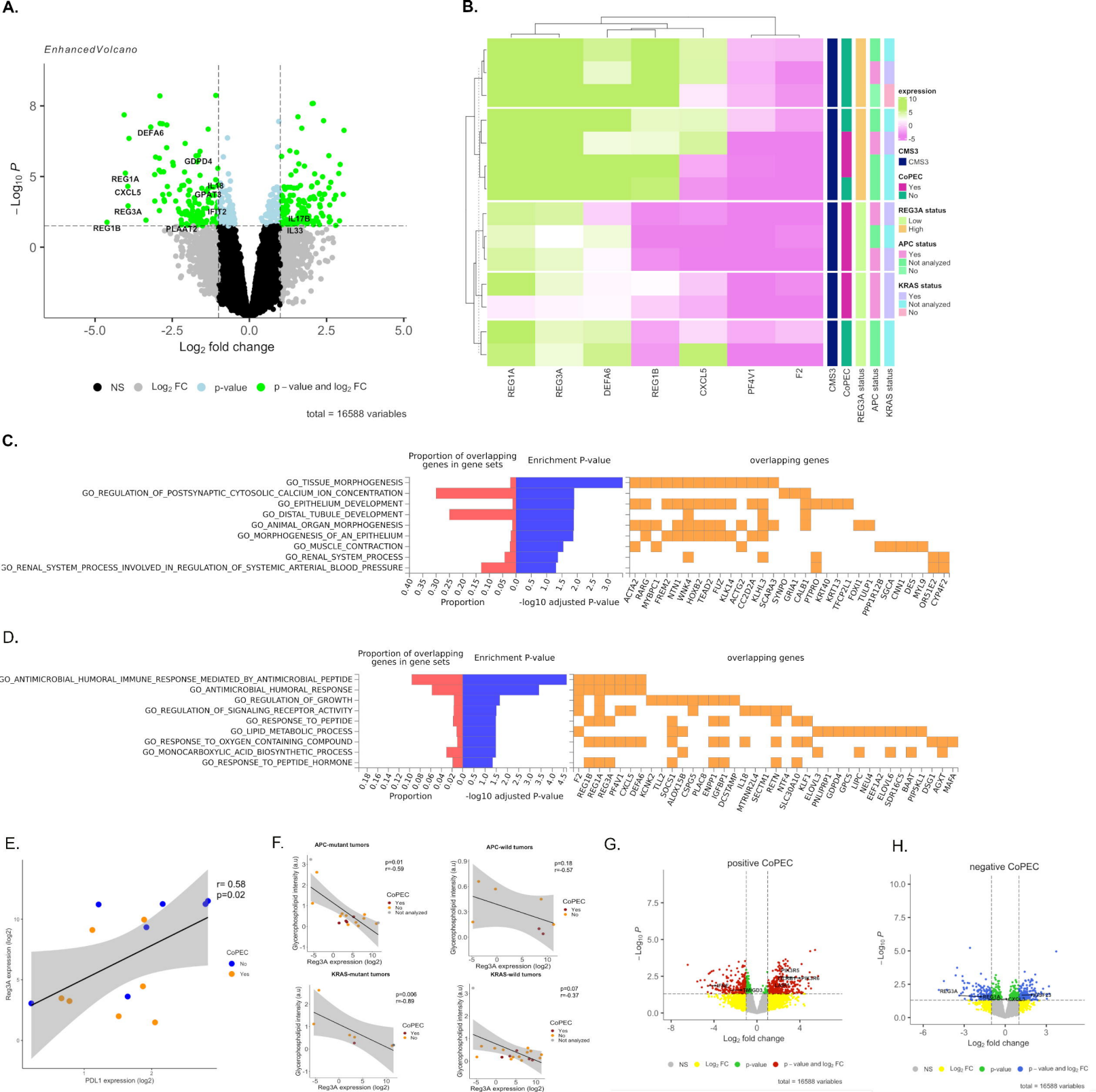
A.
EnhancedVolcano
DEFA6
GDPD4
REG1A
CXCL5
REG3A
REG1B
IL18
GPAT3
TFIT2
PLAAT2
IL17B
IL33
−Log10 P
Log2 fold change
NS
Log2 FC
p-value
p – value and log2 FC
total = 16588 variables
B.
expression
CMS3
CoPEC
REG3A status
APC status
KRAS status
REG1A
REG3A
DEFA6
REG1B
CXCL5
PF4V1
F2
C.
Proportion of overlapping genes in gene sets
Enrichment P-value
overlapping genes
GO_TISSUE_MORPHOGENESIS
GO_REGULATION_OF_POSTSYNAPTIC_CYTOSOLIC_CALCIUM_ION_CONCENTRATION
GO_EPITHELIUM_DEVELOPMENT
GO_DISTAL_TUBULE_DEVELOPMENT
GO_ANIMAL_ORGAN_MORPHOGENESIS
GO_MORPHOGENESIS_OF_AN_EPITHELIUM
GO_MUSCLE_CONTRACTION
GO_RENAL_SYSTEM_PROCESS
GO_RENAL_SYSTEM_PROCESS_INVOLVED_IN_REGULATION_OF_SYSTEMIC_ARTERIAL_BLOOD_PRESSURE
Proportion
-log10 adjusted P-value
D.
Proportion of overlapping genes in gene sets
Enrichment P-value
overlapping genes
GO_ANTIMICROBIAL_HUMORAL_IMMUNE_RESPONSE_MEDIATED_BY_ANTIMICROBIAL_PEPTIDE
GO_ANTIMICROBIAL_HUMORAL_RESPONSE
GO_REGULATION_OF_GROWTH
GO_REGULATION_OF_SIGNALING_RECEPTOR_ACTIVITY
GO_RESPONSE_TO_PEPTIDE
GO_LIPID_METABOLIC_PROCESS
GO_RESPONSE_TO_OXYGEN_CONTAINING_COMPOUND
GO_MONOCARBOXYLIC_ACID_BIOSYNTHETIC_PROCESS
GO_RESPONSE_TO_PEPTIDE_HORMONE
Proportion
-log10 adjusted P-value
E.
r= 0.58
p=0.02
CoPEC
No
Yes
Reg3A expression (log2)
PDL1 expression (log2)
F.
APC-mutant tumors
APC-wild tumors
KRAS-mutant tumors
KRAS-wild tumors
Glycerophospholipid intensity (a.u)
Reg3A expression (log2)
CoPEC
Yes
No
Not analyzed
G.
positive CoPEC
−Log10 P
Log2 fold change
NS
Log2 FC
p-value
p – value and log2 FC
total = 16588 variables
H.
negative CoPEC
−Log10 P
Log2 fold change
NS
Log2 FC
p-value
p – value and log2 FC
total = 16588 variables

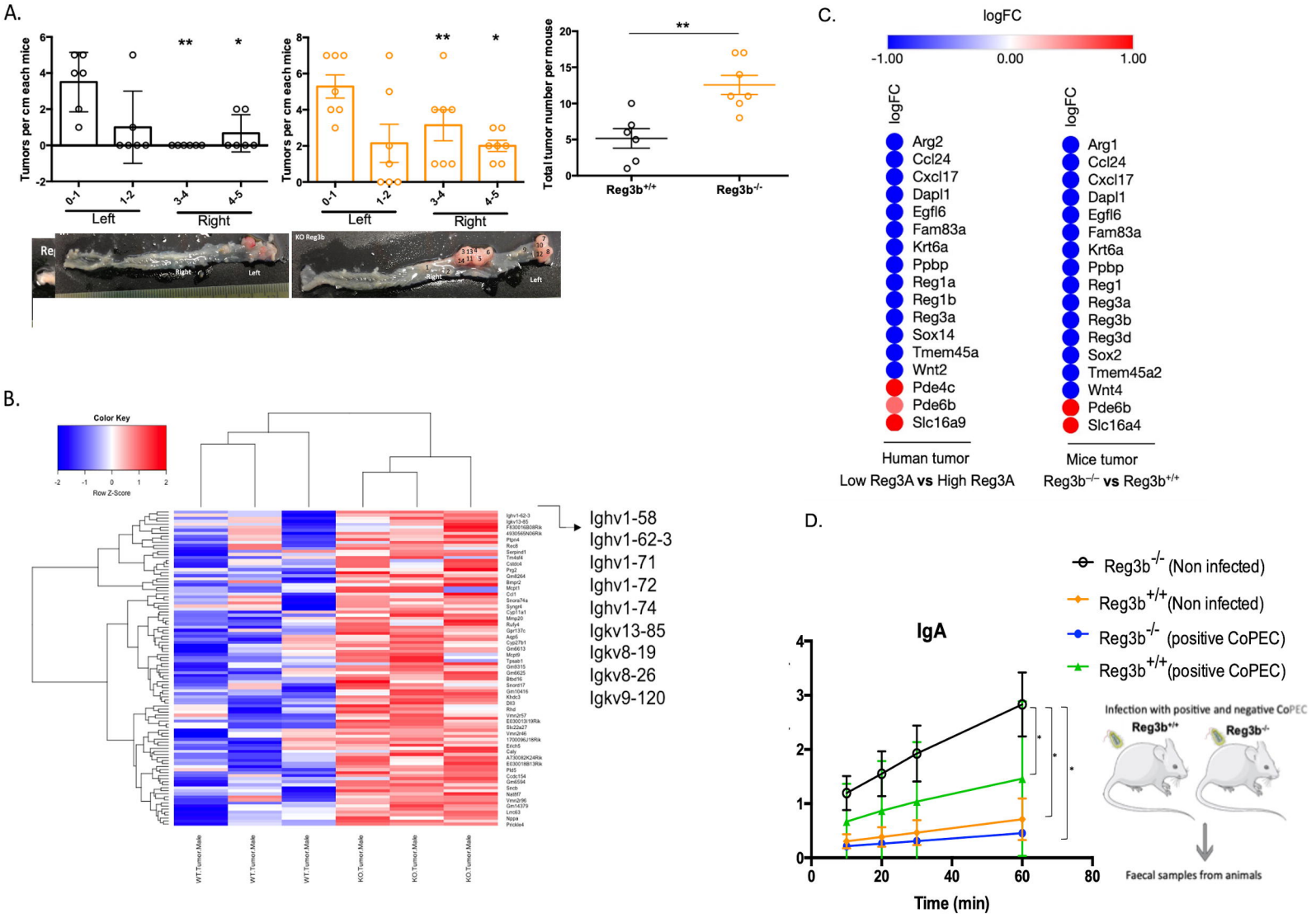
A.
Tumors per cm each mice
0-1
1-2
3-4
4-5
Left
Right
Total tumor number per mouse
Reg3b+/+
Reg3b-/-
KO Reg3b
B.
Color Key
Row Z-Score
Ighv1-58
Ighv1-62-3
Ighv1-71
Ighv1-72
Ighv1-74
Igkv13-85
Igkv8-19
Igkv8-26
Igkv9-120
C.
logFC
-1.00
0.00
1.00
Arg2
Ccl24
Cxcl17
Dapl1
Egfl6
Fam83a
Krt6a
Ppbp
Reg1a
Reg1b
Reg3a
Sox14
Tmem45a
Wnt2
Pde4c
Pde6b
Slc16a9
Human tumor
Low Reg3A vs High Reg3A
Arg1
Ccl24
Cxcl17
Dapl1
Egfl6
Fam83a
Krt6a
Ppbp
Reg1
Reg3a
Reg3b
Reg3d
Sox2
Tmem45a2
Wnt4
Pde6b
Slc16a4
Mice tumor
Reg3b−/− vs Reg3b+/+
D.
IgA
Reg3b-/- (Non infected)
Reg3b+/+ (Non infected)
Reg3b-/- (positive CoPEC)
Reg3b+/+ (positive CoPEC)
Time (min)
Infection with positive and negative CoPEC
Reg3b+/+
Reg3b-/-
Faecal samples from animals

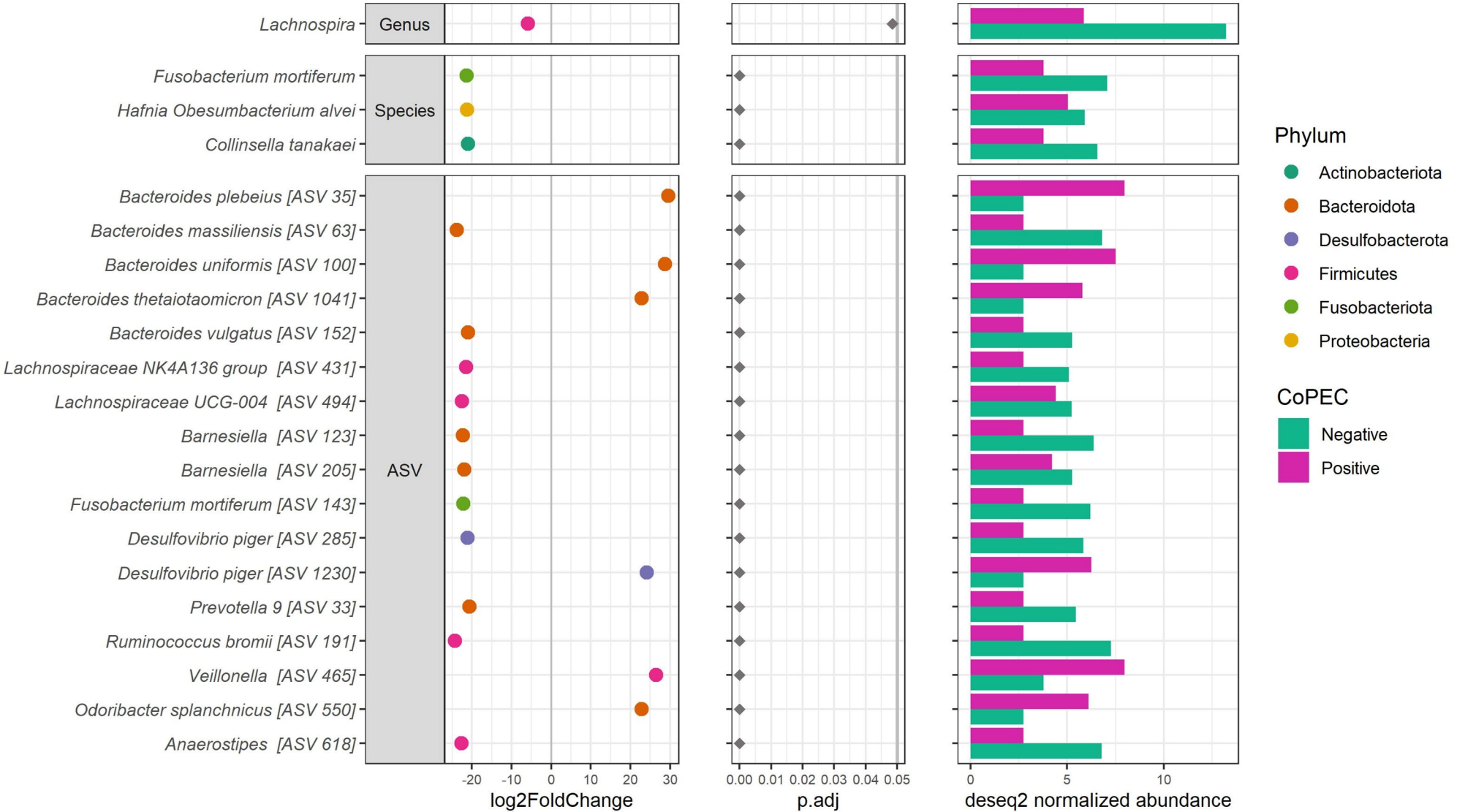
Lachnospira
Genus
Fusobacterium mortiferum
Hafnia Obesumbacterium alvei
Collinsella tanakaei
Species
Bacteroides plebeius [ASV 35]
Bacteroides massiliensis [ASV 63]
Bacteroides uniformis [ASV 100]
Bacteroides thetaiotaomicron [ASV 1041]
Bacteroides vulgatus [ASV 152]
Lachnospiraceae NK4A136 group [ASV 431]
Lachnospiraceae UCG-004 [ASV 494]
Barnesiella [ASV 123]
Barnesiella [ASV 205]
Fusobacterium mortiferum [ASV 143]
Desulfovibrio piger [ASV 285]
Desulfovibrio piger [ASV 1230]
Prevotella 9 [ASV 33]
Ruminococcus bromii [ASV 191]
Veillonella [ASV 465]
Odoribacter splanchnicus [ASV 550]
Anaerostipes [ASV 618]
ASV
-20 -10 0 10 20 30
log2FoldChange
0.00 0.01 0.02 0.03 0.04 0.05
p.adj
0 5 10
deseq2 normalized abundance
Phylum
Actinobacteriota
Bacteroidota
Desulfobacterota
Firmicutes
Fusobacteriota
Proteobacteria
CoPEC
Negative
Positive

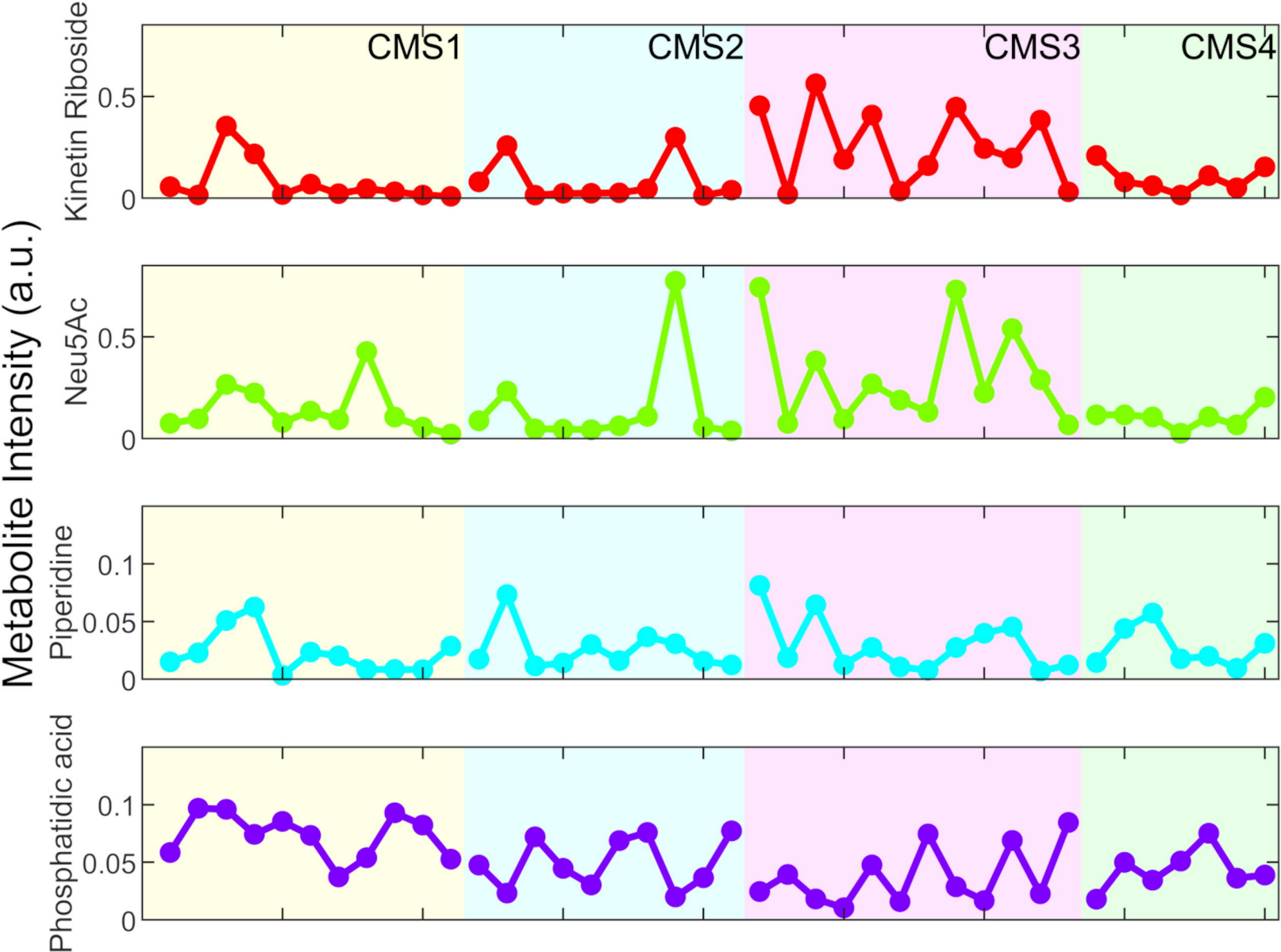
Metabolite Intensity (a.u.)
CMS1
CMS2
CMS3
CMS4
Kinetin Riboside
0.5
0
Neu5Ac
0.5
0
Piperidine
0.1
0.05
0
Phosphatidic acid
0.1
0.05
0

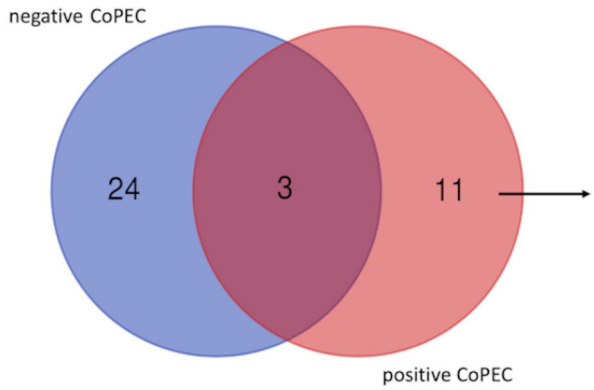
negative CoPEC
24
3
11
positive CoPEC

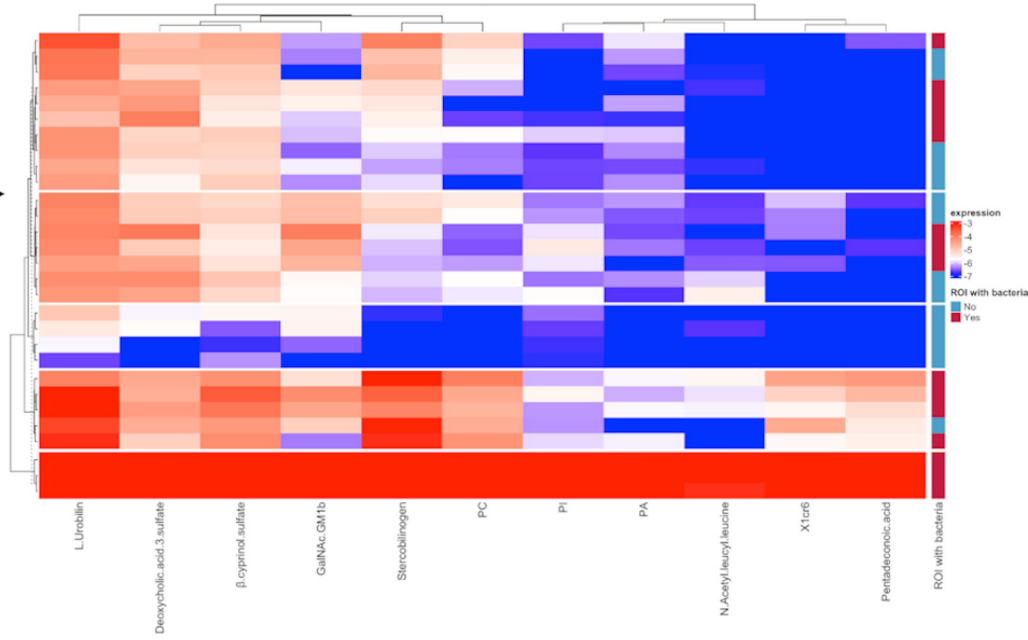
expression
-3
-4
-5
-6
-7
ROI with bacteria
No
Yes
L.Urobilin
Deoxycholic.acid.3.sulfate
β.cyprinol.sulfate
GalNAc.GM1b
Stercobilinogen
PC
PI
PA
N.Acetyl.leucyl.leucine
X1cr6
Pentadeconoic.acid
ROI with bacteria